# The novel ribosome biogenesis inhibitor usnic acid blocks nucleolar pre-60S maturation

## Supplementary Information

**Source data of Supplementary Information are provided with this paper.**

Lisa Kofler[1*], Lorenz Emanuel Grundmann[2,3*], Magdalena Gerhalter[1], Michael Prattes[1], Juliane Merl-Pham[4], Gertrude Zisser[1], Irina Grishkovskaya[2], Victor-Valentin Hodirnau[5], Martin Vareka[6], Rolf Breinbauer[6], Stefanie M. Hauck[4], David Haselbach[2] and Helmut Bergler[1]

[1] Institute of Molecular Biosciences, University of Graz, Graz, 8010, Austria
[2] Research Institute of Molecular Pathology (IMP), Vienna BioCenter, Vienna, 1030, Austria
[3] Vienna BioCenter PhD Program, Doctoral School of the University of Vienna and Medical 10 University of Vienna, 1030, Vienna, Austria
[4] Metabolomics and Proteomics Core, Helmholtz Center Munich, German Center for Environmental Health GmbH, D-80939, Germany
[5] Institute of Science and Technology Austria, Klosterneuburg, Austria
[6] Institute of Organic Chemistry, Graz University of Technology, Stremayrgasse 9, Graz, 8010, Austria

Correspondence should be addressed to helmut.bergler@uni-graz.at or david.haselbach@imp.ac.at

***These authors contributed equally.**

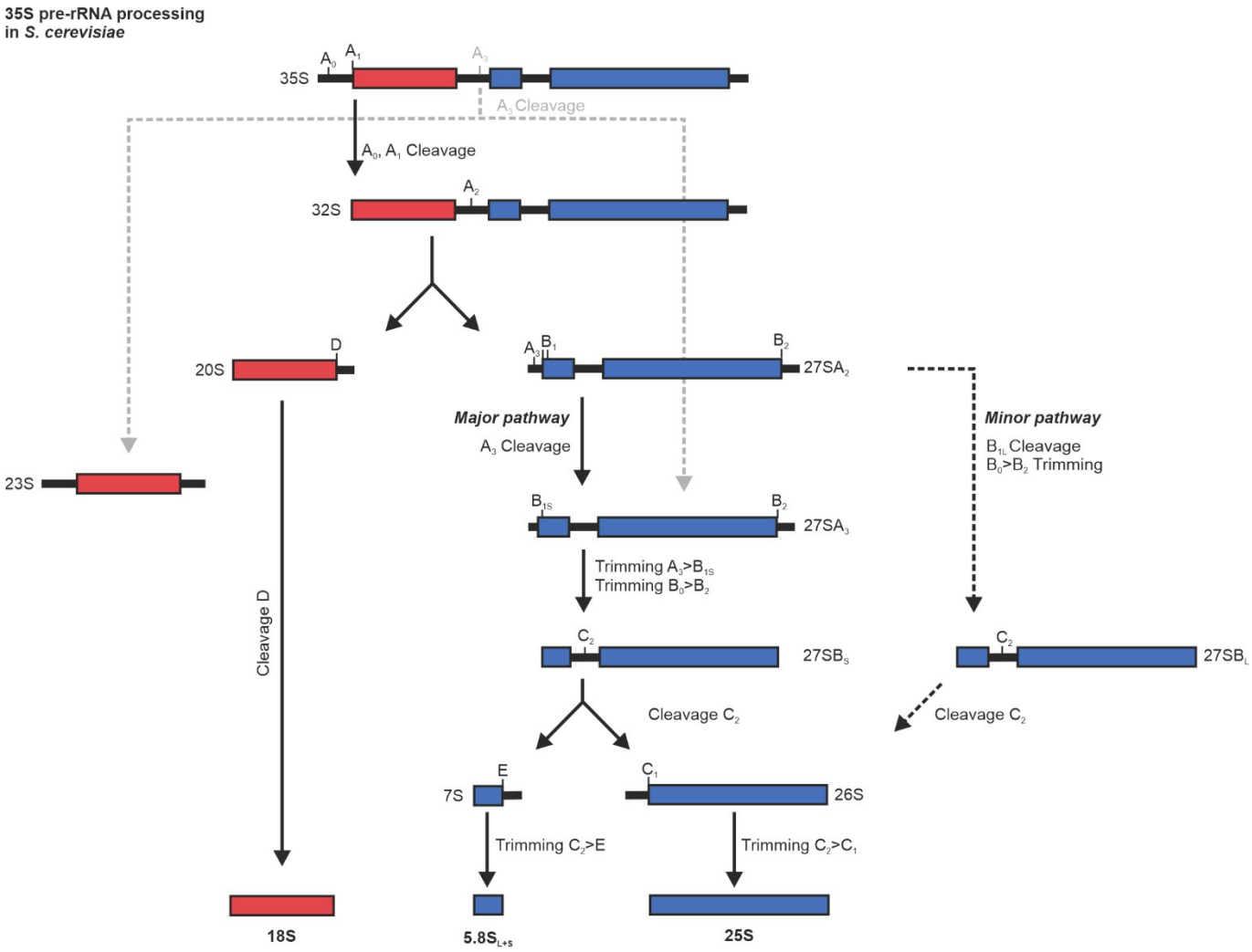


Supplementary Fig. 1. **Schematic overview of eucaryotic 35S pre-rRNA processing in yeast.** Pol I transcribes the 35S pre-rRNA that enters a sophisticated processing pathway of exo- and endonucleolytic cleavage reactions. Internal and external spacer segments are removed generating the mature ends of the ribosomal RNAs (18S, 25S, 5.8S; 5S rRNA is transcribed separately by Pol III). If cleavage at sites $A_0$ to $A_2$ are inhibited, $A_3$ cleavage can take place (indicated in grey dashed lines) leading to aberrant 23S pre-rRNA and $27SA_3$ pre-rRNA.

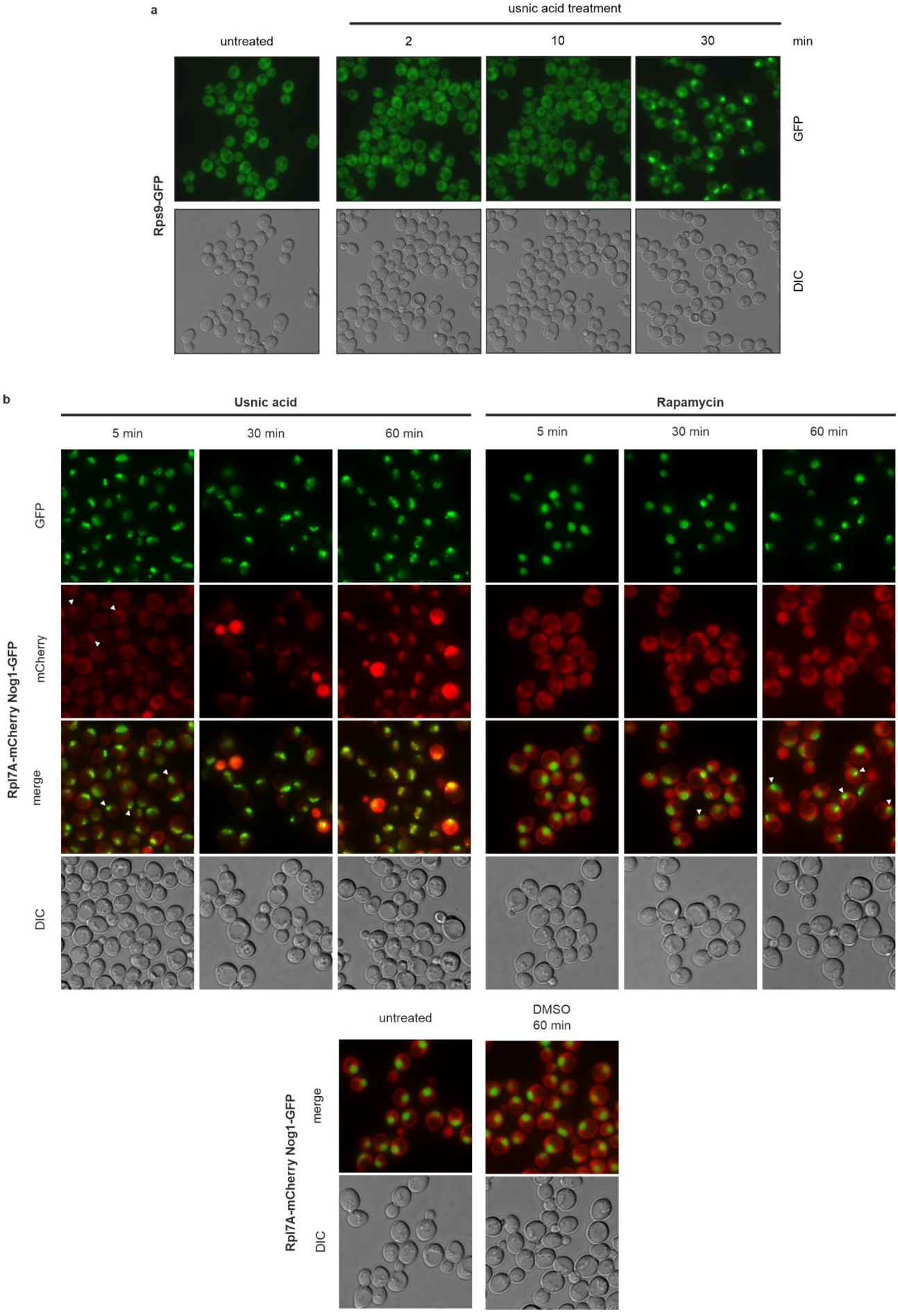
a
usnic acid treatment
untreated
2
10
30
min
Rps9-GFP
GFP
DIC
b
Usnic acid
Rapamycin
5 min
30 min
60 min
5 min
30 min
60 min
Rpl7A-mCherry Nog1-GFP
GFP
mCherry
merge
DIC
untreated
DMSO
60 min
Rpl7A-mCherry Nog1-GFP
merge
DIC

Supplementary Fig. 2 (previous page). **Usnic acid targets maturation of the large ribosomal subunit.** **a** Kinetics of usnic acid effects on small subunit maturation. Nuclear accumulation of the 40S reporter strain Rps9-GFP [1] occurs only after 30 minutes of incubation with usnic acid. **b** Usnic acid does not exert its effects on ribosome biogenesis through inhibition of TORC1. The Rpl7-mCherry Nog1-GFP strain was treated either with usnic acid or the TORC1 inhibitor rapamycin. While Nog1-GFP showed nucleolar accumulation (white triangles) within 5 minutes of usnic acid treatment, it required 30 to 60 minutes of rapamycin treatment. Moreover, Rpl7-mCherry accumulates in the nucleus of usnic acid treated cells, but stays in the cytosol in rapamycin treated cells. Cells untreated or treated with DMSO, the solvent of rapamycin, served as controls.

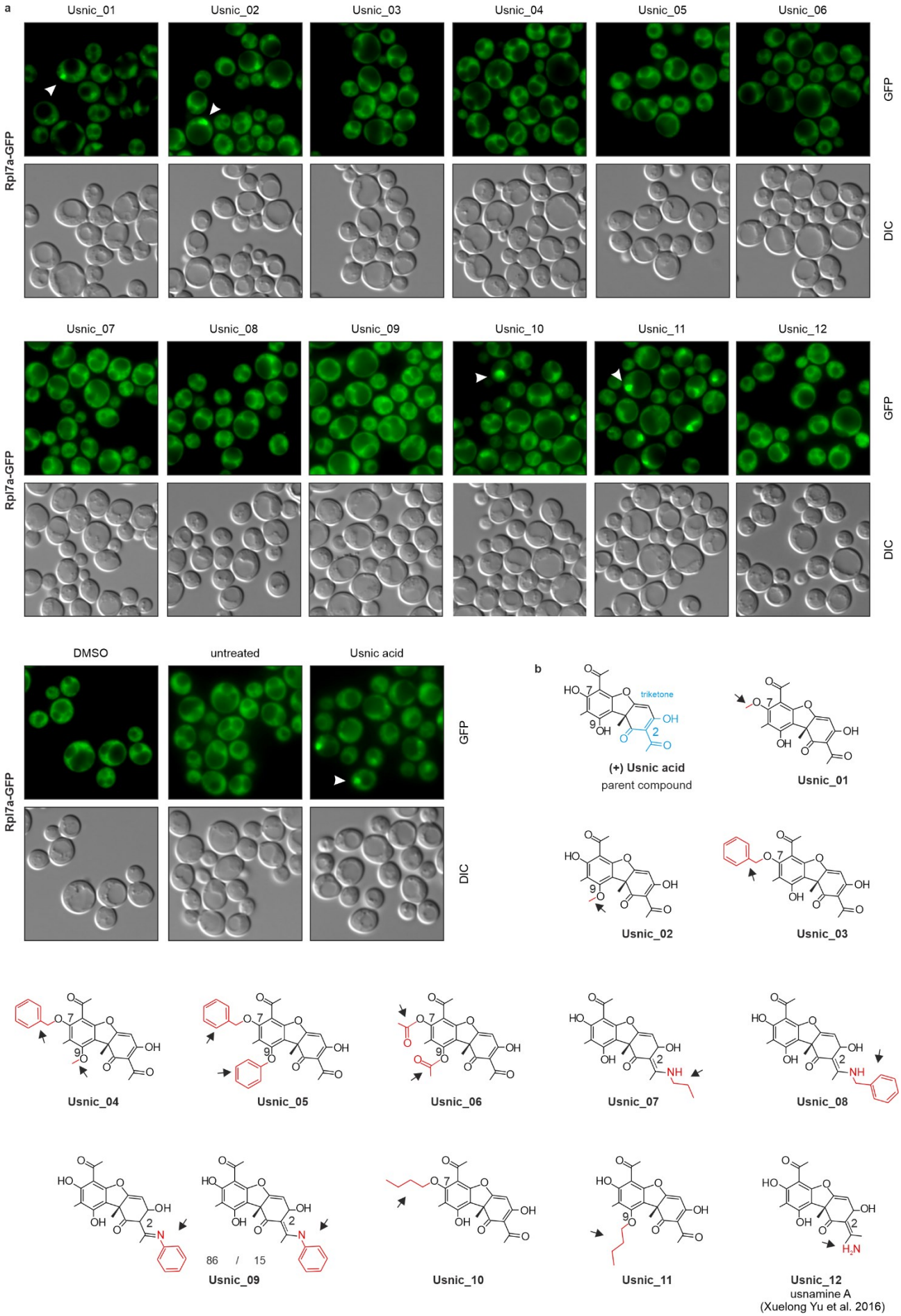
a
Usnic_01
Usnic_02
Usnic_03
Usnic_04
Usnic_05
Usnic_06
Rpl7a-GFP
GFP
DIC
Usnic_07
Usnic_08
Usnic_09
Usnic_10
Usnic_11
Usnic_12
DMSO
untreated
Usnic acid
b
triketone
(+) Usnic acid
parent compound
Usnic_01
Usnic_02
Usnic_03
Usnic_04
Usnic_05
Usnic_06
Usnic_07
Usnic_08
Usnic_09
Usnic_10
Usnic_11
Usnic_12
usnamine A
(Xuelong Yu et al. 2016)

Supplementary Fig. 3 (previous page). **New usnic acid derivatives tested for their inhibitory effect on ribosome biogenesis. a** The derivatives Usnic_1-12 were tested for their inhibitory effect on ribosome biogenesis by fluorescence microscopy of the Rpl7a-GFP reporter strain[1]. The cells were treated for 10 minutes with 60 µM of each compound dissolved in DMSO. As control, the parent compound was also solved in DMSO. A clear nuclear accumulation was only observed for derivatives 1, 2, 10 and 11. **b** Chemical structures of the parent compound (+)-usnic acid and its newly synthesized derivatives. The triketone moiety of the parent compound is highlighted in blue. The different modifications at positions 2, 7 and/or 9 are highlighted in red and indicated by an arrow.

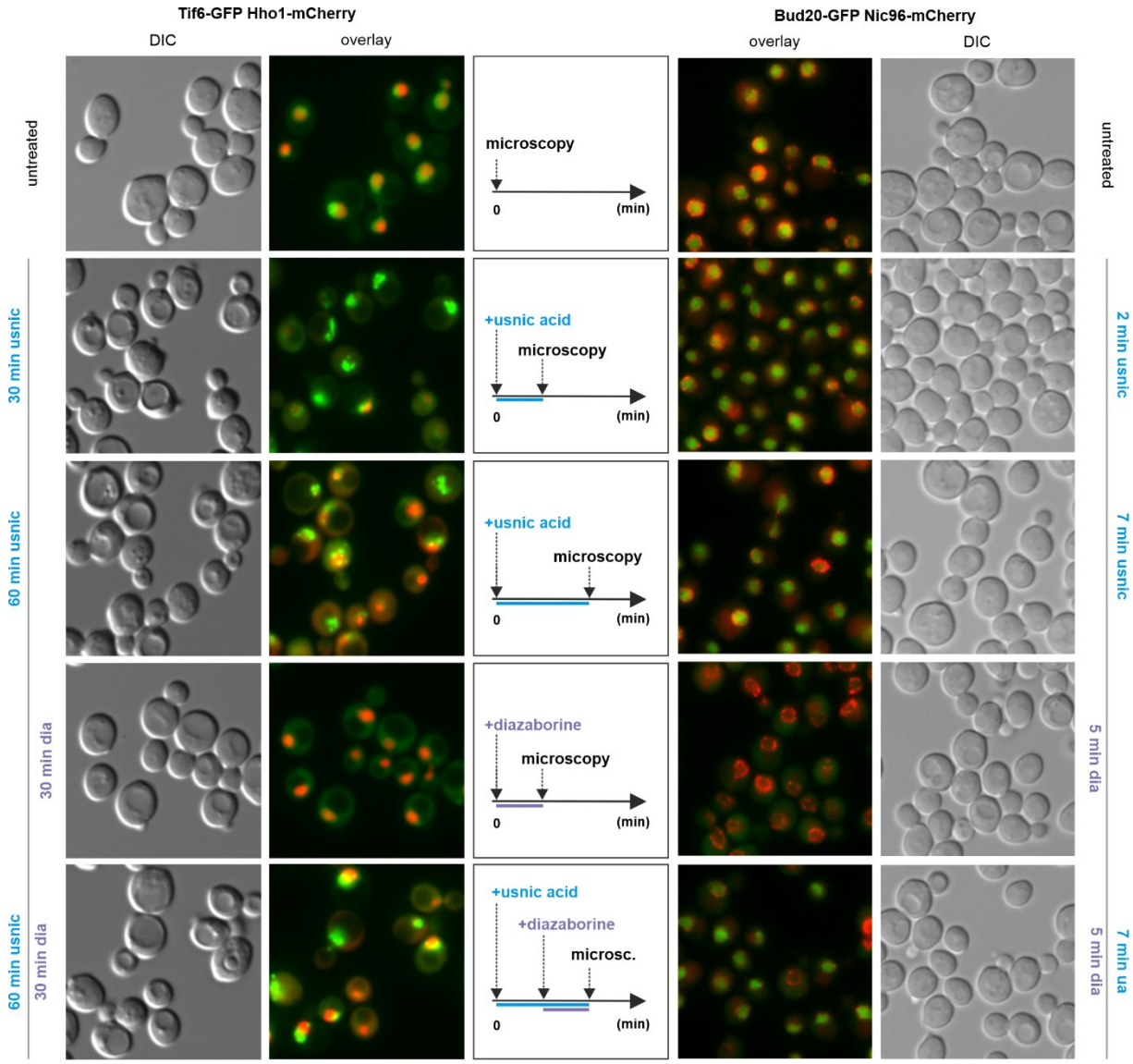


Supplementary Fig. 4. **Usnic acid treatment traps Bud20- and Tif6-GFP in the nucleus.** Wildtype cells chromosomally expressing the GFP-tagged shuttling factors Bud20 or Tif6 were treated with usnic acid (40 µM), diazaborine (10 µg/ml) or both inhibitors, as indicated. The localization of the proteins was examined by fluorescence microscopy. Untreated cells served as control. Nic96-mCherry served as nuclear membrane marker, Hho1-mCherry as marker for the nucleoplasm. As reported previously[2], diazaborine treatment shifted Bud20-GFP and Tif6-GFP to the cytoplasm. In contrast, treatment with usnic acid led to an entrapment of these shuttling factors in the nucleus. Pretreatment with usnic acid blocked the shift of the GFP-signal to the cytoplasm upon diazaborine treatment.

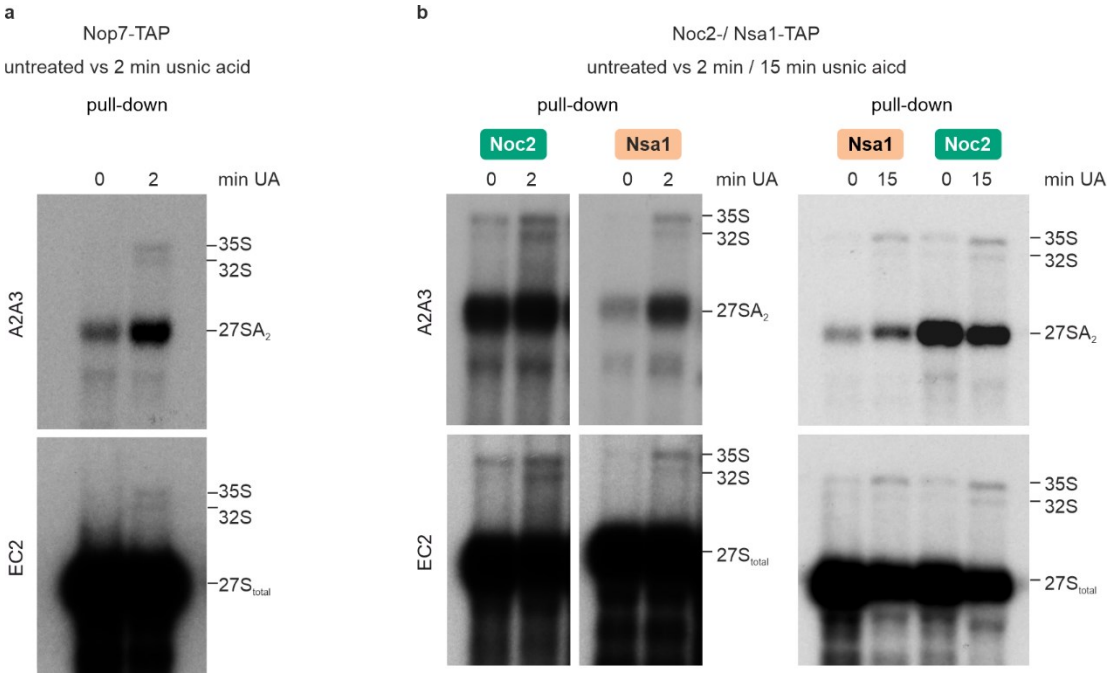


Supplementary Fig. 5. **Nop7-TAP, Nsa1-TAP and Noc2-TAP purifications contain mainly 27SB and little $27SA_2$ pre-rRNA.** Northern blots using the EC2 and A2A3 probes were exposed to show roughly the same intensities for 32S and 35S pre-rRNA. Detected (pre)-rRNA species are marked on the right, the probes used are indicated on the left. **a** Northern blot with RNAs isolated from Nop7-TAP purifications after two minutes of treatment with usnic acids. **b** Northern blots with RNAs isolated from Noc2-TAP and Nsa1-TAP purifications after 2 minutes and 15 minutes of usnic acid treatment. RNAs isolated from TAP-purifications from the untreated strains served as controls (0).

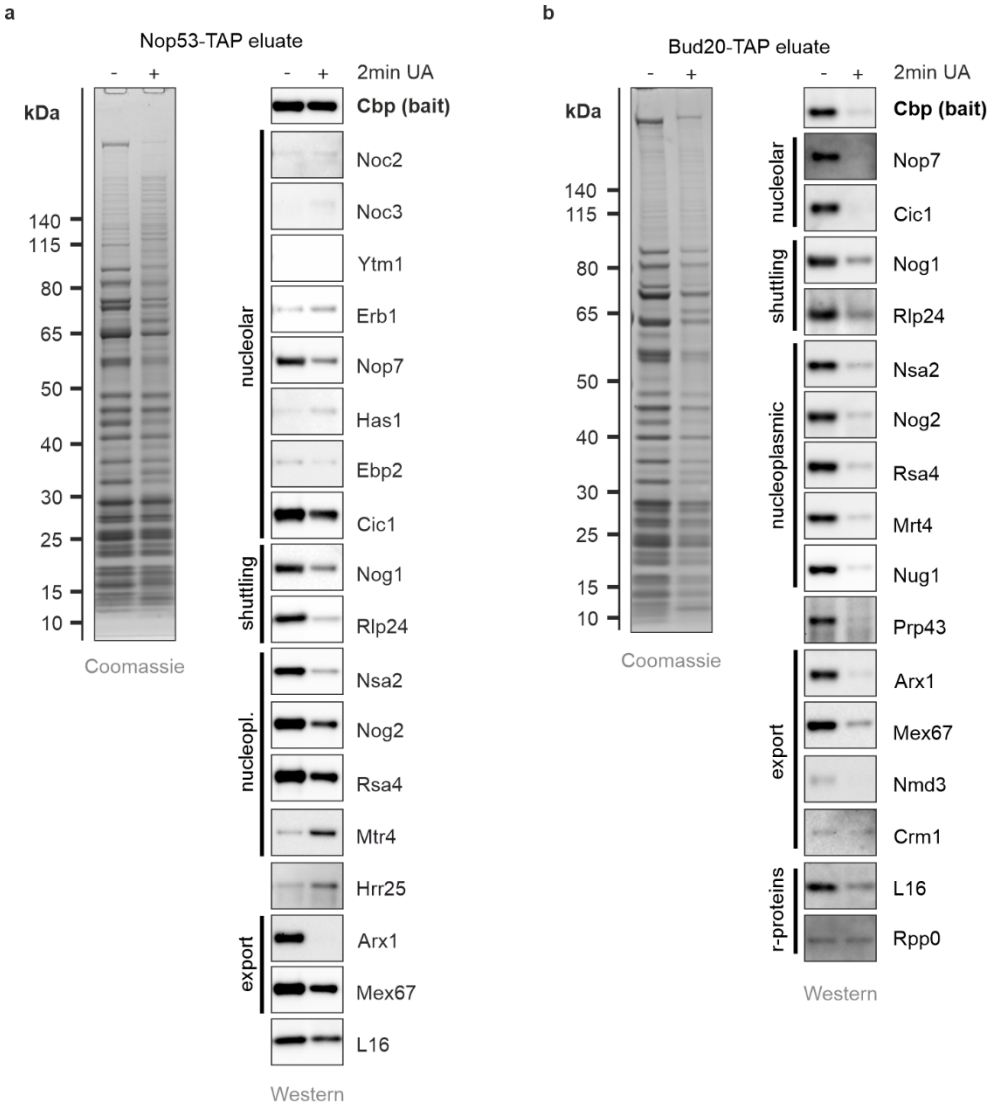


Supplementary Fig. 6. **The assembly factors Nop53 (a) and Bud20 (b) cannot bind to the maturing pre-60S particle in the presence of usnic acid.** Nop53-TAP and Bud20-TAP were isolated from untreated cells (-) or cells treated for 2 minutes with 60 µM usnic acid (+). The protein content of the purified particles was analyzed via SDS-PAGE followed by Coomassie staining or Western blotting.

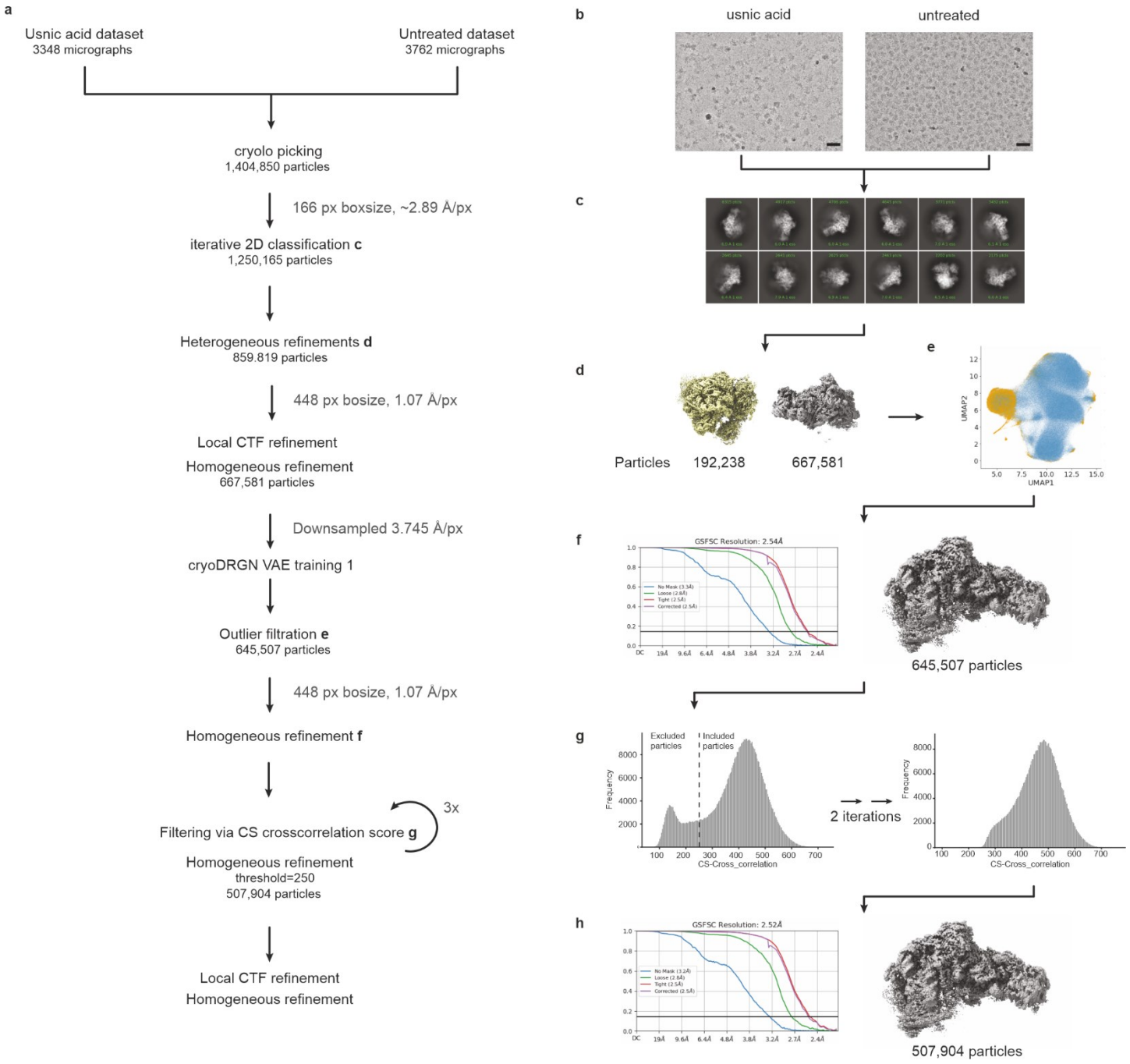


Supplementary Fig. 7. **Single-particle cryo-EM preprocessing workflow. a** Overview of the workflow. **b** Micrographs for 2 min usnic acid treated and untreated samples were combined for pre-processing. After particle picking using crYOLO, particles were extracted with a box size of 448 binned to 166. **c** 2D classification was followed by **d** ab initio modeling and further cleaning of the particle stack by iterative heterogeneous refinements, followed by local CTF refinement and homogeneous refinement. **e** For a first cryoDRGN analysis, downsampled particles (3.745 Å/pixel) were used for training of the network with a latent variable of 10 dimensions for 50 epochs. Ice-contaminated and outlier particles were filtered via thresholding of their latent space Eigenvektor values. Excluded particles are shown in orange. **f** Particles were reimported to cryoSPARC and refined. **g** Poorly resolving and aligning particles were excluded by excluding particles with a CryoSparc_cross_correlation value below 250. This was repeated twice while refining the including particles in each iteration. **h** The final particle stack was subjected to local CTF refinement and homogeneous refinement.

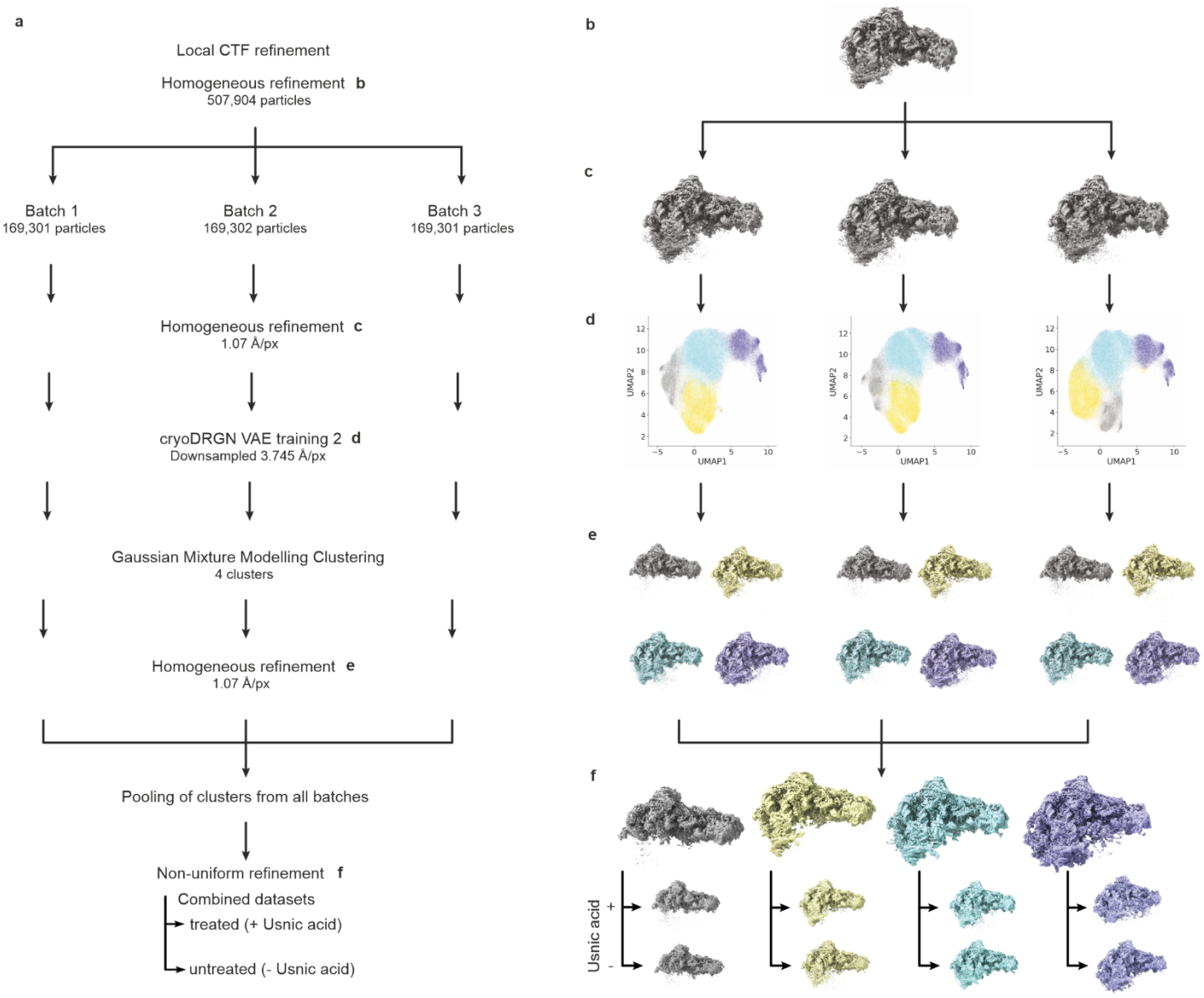


Supplementary Fig. 8. **CryoDRGN and clustering workflow. a** Overview of the final processing steps continuing the workflow shown in figure S7. **b** The final particle stack was subjected to local CTF refinement and homogeneous refinement. **c** Particles were randomly split into three stacks and refined in cryoSPARC and **d** used for another round of cryoDRGN analysis with a latent variable of 8 dimensions. Particles were clustered using a Gaussian-Mixture Model on the cryoDRGN latent space embeddings with a rand. **e** Clusters were refined in cryoSPARC. **f** Structurally identical clusters of each batch were combined and refined. Further, each combined cluster was separated into particles originating from the treated and untreated dataset and refined. Maps were post-processed using DeepEMhancer.

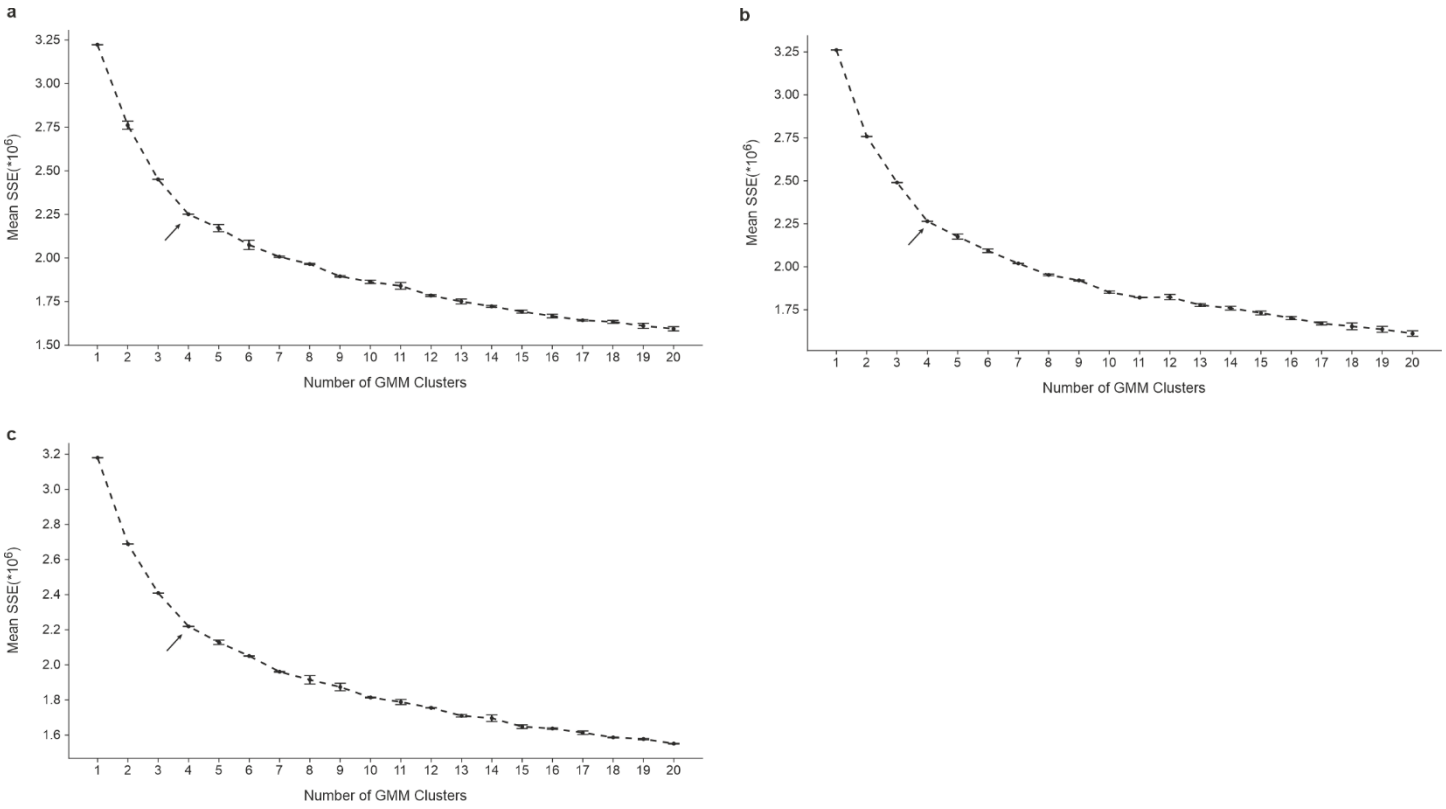


Supplementary Fig. 9. **Elbow analysis for Gaussian mixture modelling (GMM).** Latent variables for batches 1, 2 and 3 (**a**, **b** and **c** respectively) were clustered using GMM with 1 to 20 clusters and a randomly generated seed. This was repeated thrice. For each clustering the sum of squared errors (SSE) was calculated and averaged over all iterations. Error bars indicate respective standard deviations. Arrows indicate the “elbow” at 4 clusters in every batch.

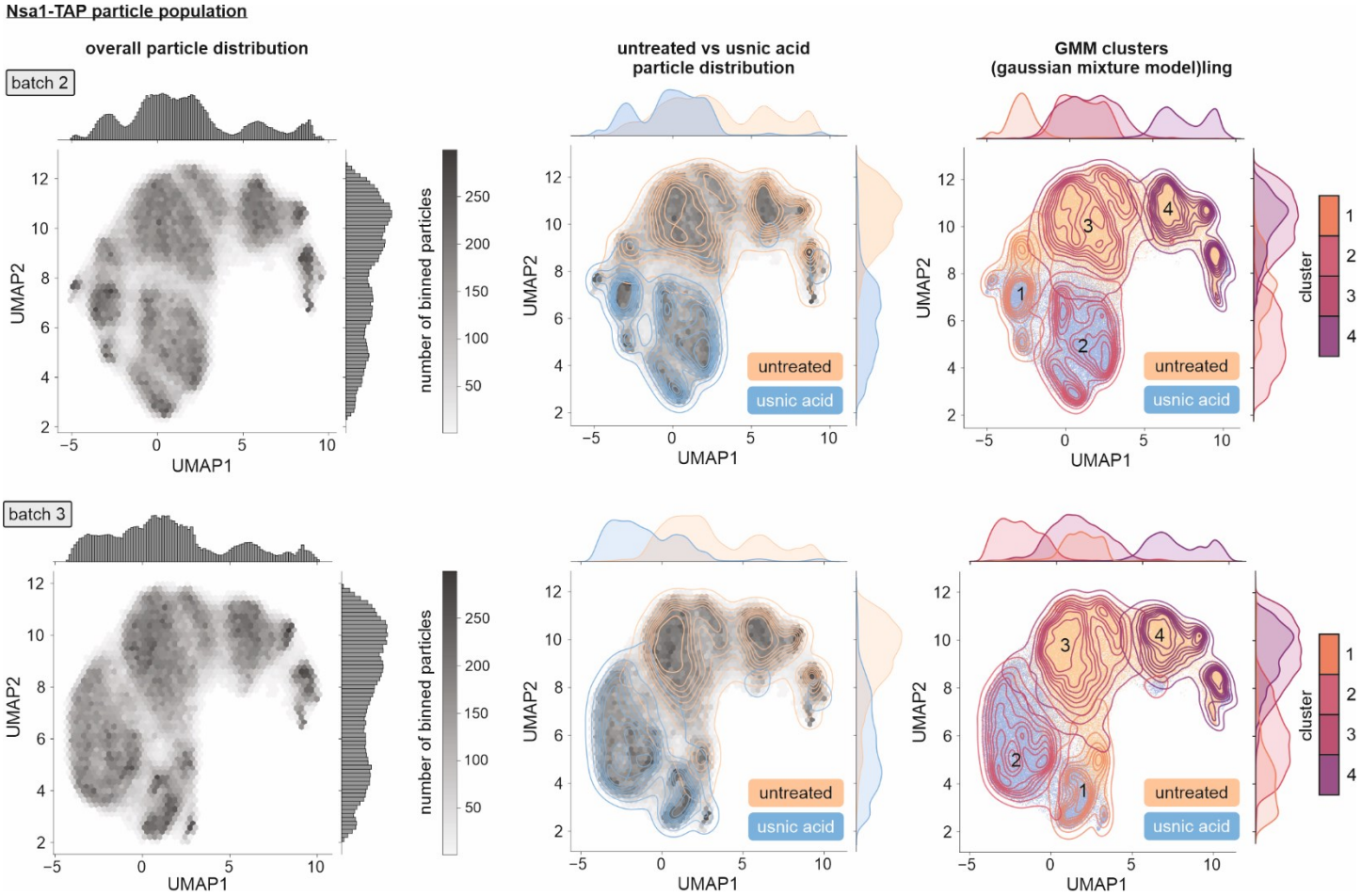


Supplementary Fig. 10. **cryoDRGN analysis of Nsa1-TAP batches 2 and 3.** (Batch 1 is shown in Fig. 5.) Early nucleolar 60S particles were isolated via Nsa1-TAP from untreated and 2 min usnic acid treated cells. For each sample, one single particle cryo-EM dataset was collected, and these datasets were merged for processing and quantitative analysis. (a detailed description of the data processing workflow is given in the method section and Supplementary Fig. S7 and S8). Structural heterogeneity was analyzed using cryoDRGN in three equally sized particle batches. Dimensionality reduction using UMAP and clustering using Gaussian Mixture Modelling (GMM) was performed to identify different pre-60S maturation states present in our datasets. Representative 2D UMAP projection: Of the particles' hexagonal binned 8-dimensional latent space embeddings (left). Kernel Density Estimate (kde) plot indicates particle embeddings from treated and untreated datasets (middle). Scatter plot, with each datapoint representing a single particles' embedding and kde-plots represent clusters identified using GMM (right). Numbers of binned particles are indicated in grey scale, 2 minutes usnic acid treatment in blue, untreated in yellow. The 4 clusters are represented in different shades of purple.

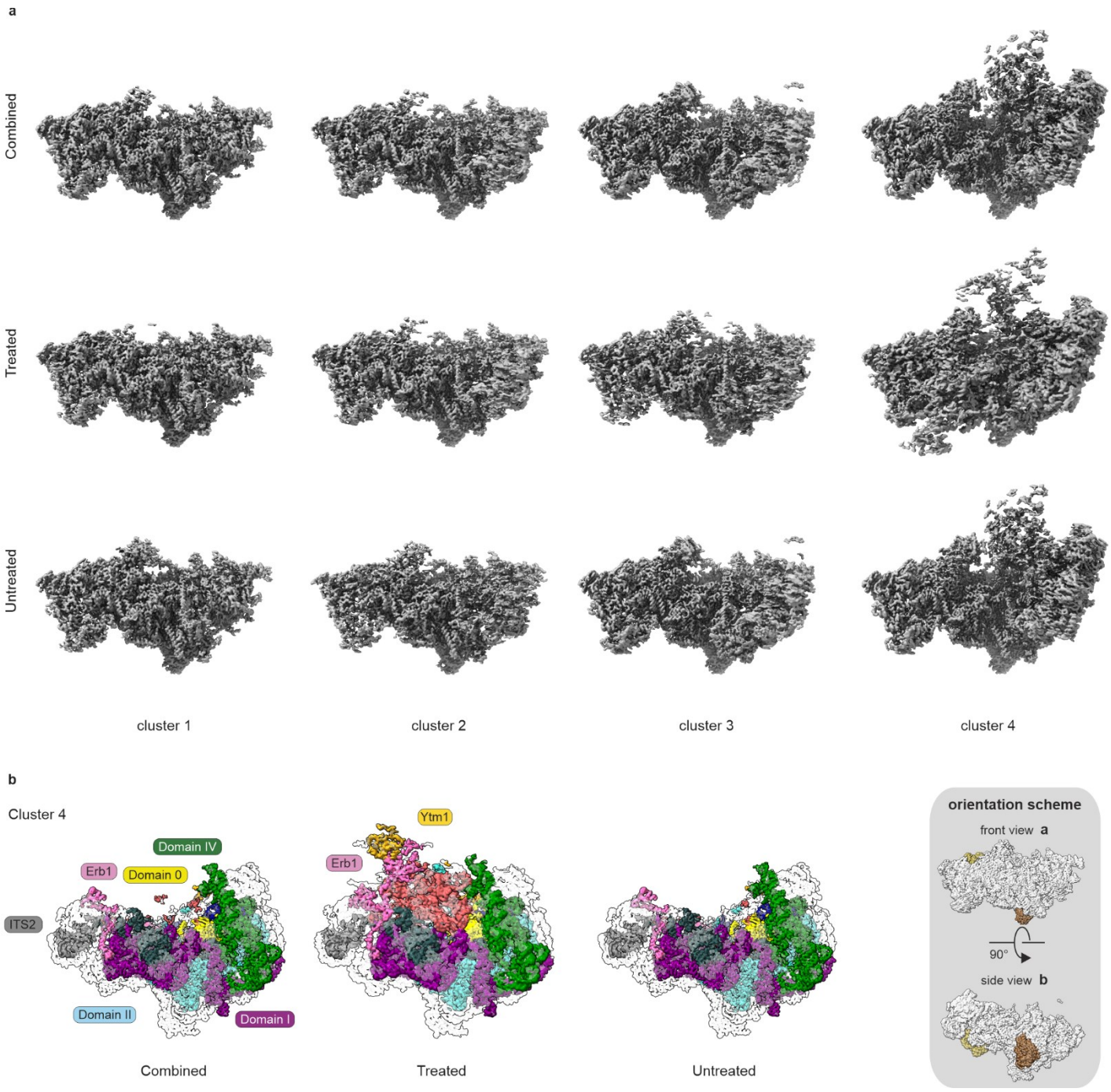


Supplementary Fig. 11. **Comparison of the total, treated and untreated clusters. a** The reconstructions of the cluster 1 to 4 originating from the combined datasets, the treated or untreated dataset. Shown are DeepEMhanced maps. **b** Cluster 4 reconstructions were rigid body fitted and colored with PDB-6EM5. Folded rRNA domains and the Erb1/Ytm1 module are indicated.

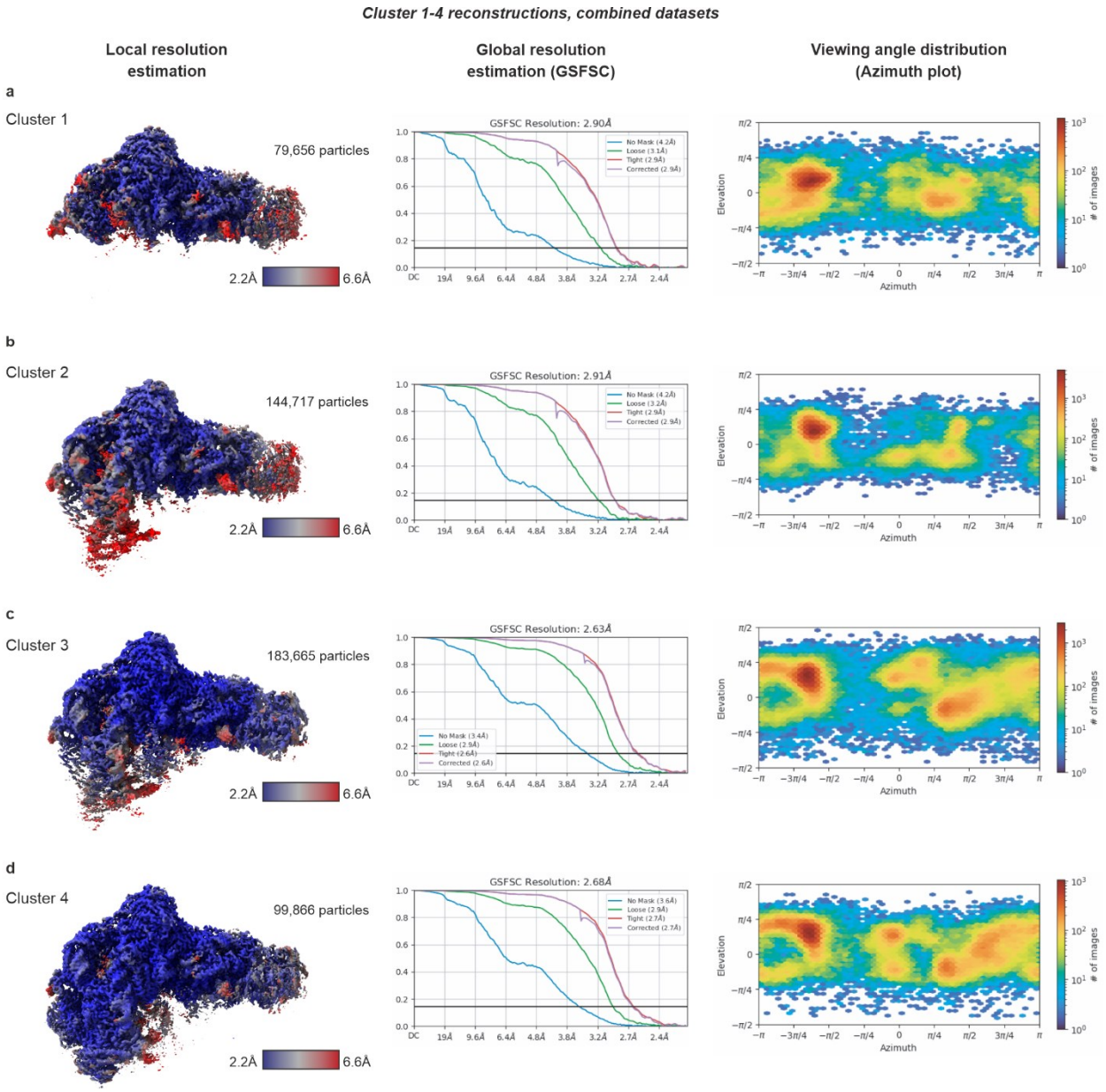


Supplementary Fig. 12. **Cryo-EM reconstructions of the combined clusters 1 to 4 (a to d).** Reconstructions colored by local resolution estimation as indicated by the color scheme. GSFSC curves for global resolution estimation are depicted and the viewing angle distribution as an Azimuth plot.

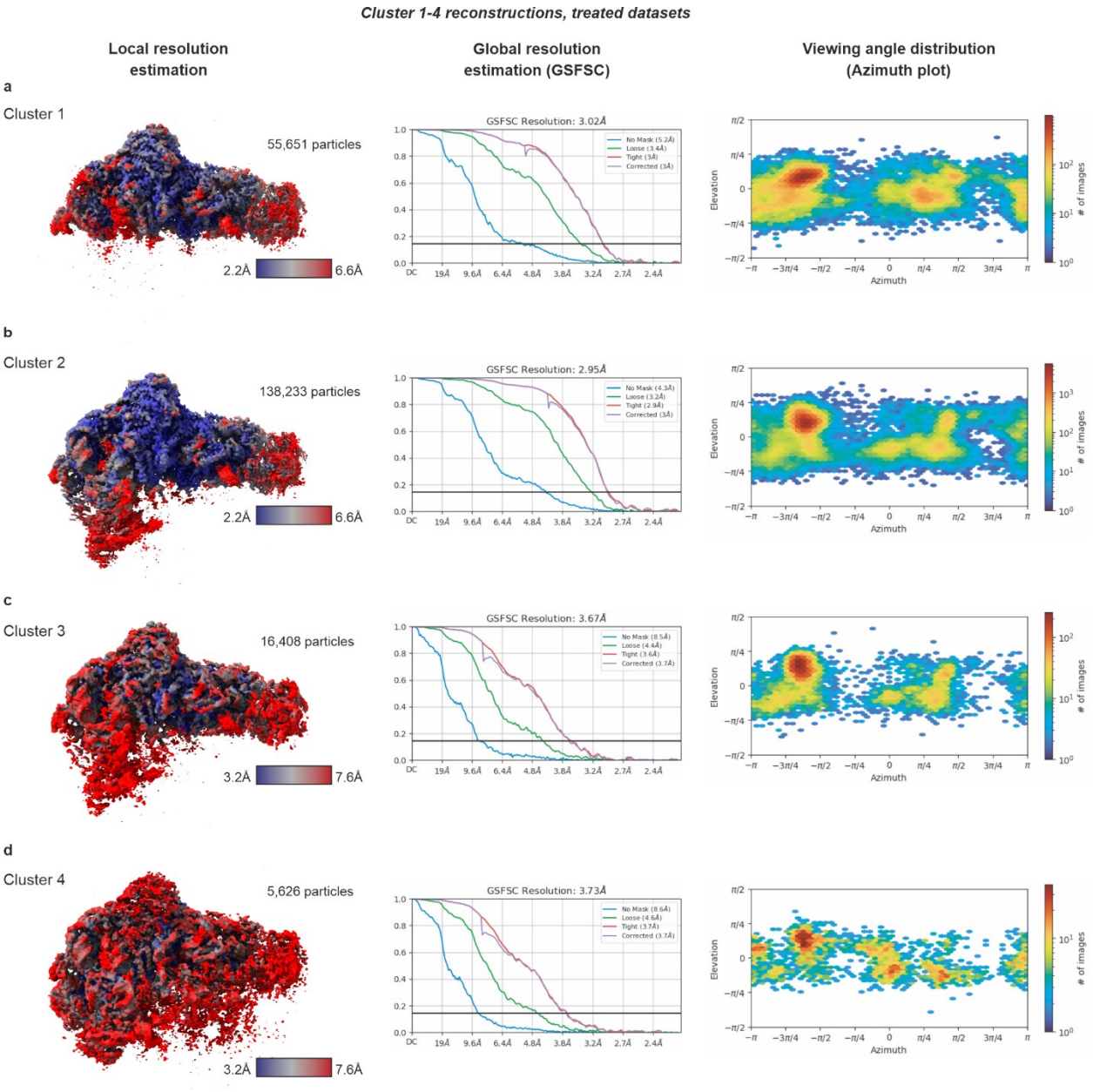


Supplementary Fig. 13. **Cryo-EM reconstructions of the treated clusters 1 to 4 (a to d).** Reconstructions colored by local resolution estimation as indicated by the color scheme. Note that the color scale differs from **a, b** to **c, d**. GSFSC curves for global resolution estimation are depicted and the viewing angle distribution as an Azimuth plot.

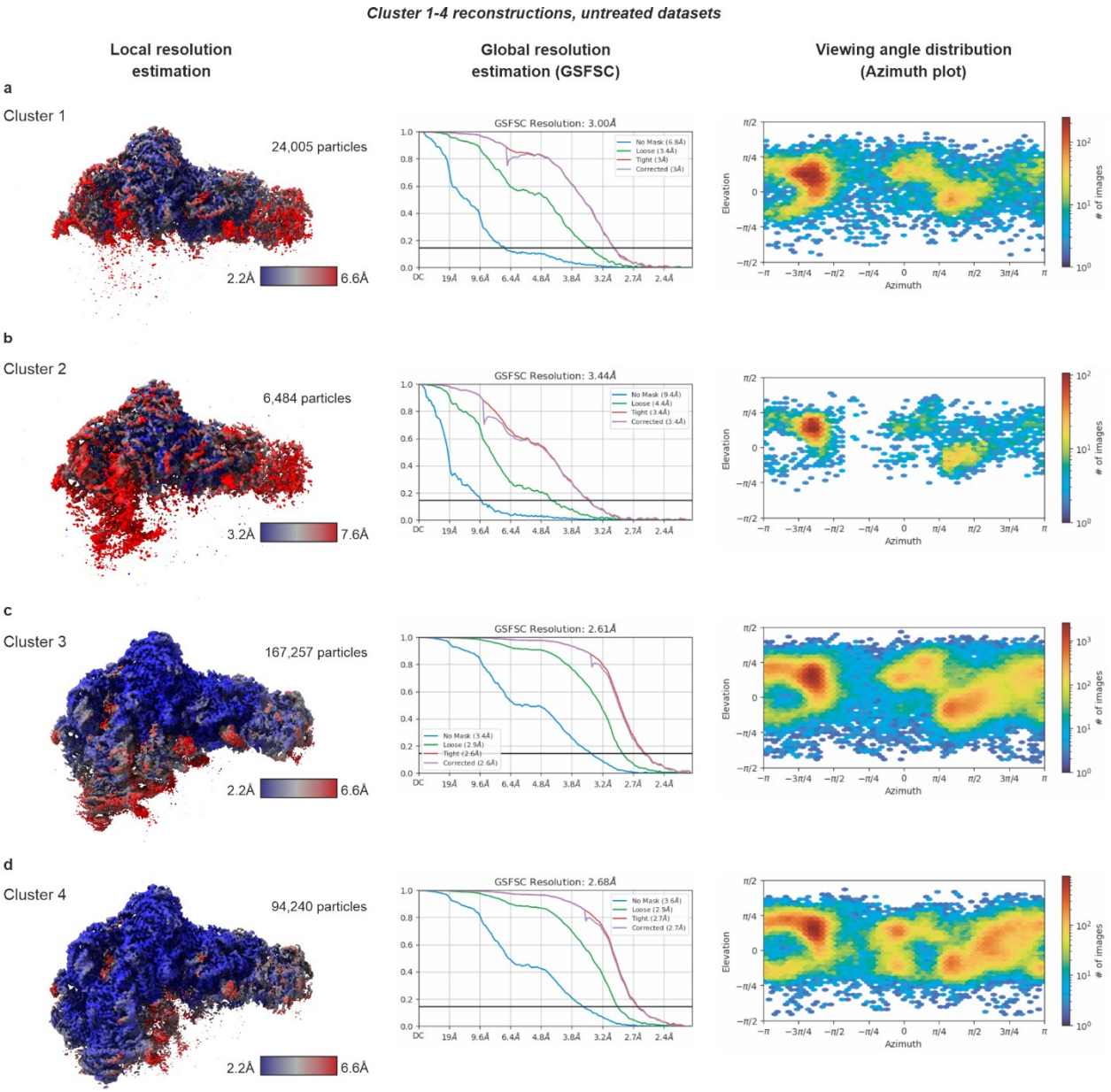


Supplementary Fig. 14. **Cryo-EM reconstructions of the untreated clusters 1 to 4 (a to d).** Reconstructions colored by local resolution estimation as indicated by the color scheme. Note that the color scale differs from **a, c, d** to **c**. GSFSC curves for global resolution estimation are depicted and the viewing angle distribution as an Azimuth plot.

**Supplementary Table 1:** usnic acid derivatives

| Name | Name UPAC | MW |
|---|---|---|
| Usnic_01 | *(R)*-1,1'-(3,9-dihydroxy-7-methoxy-8,9b-dimethyl-1-oxo-1,9b-dihydrodibenzo[b,d]furan-2,6-diyl)bis(ethan-1-one) | 358.38 g/mol |
| Usnic_02 | *(R)*-1,1'-(3,7-dihydroxy-9-methoxy-8,9b-dimethyl-1-oxo-1,9b-dihydrodibenzo[b,d]furan-2,6-diyl)bis(ethan-1-one) | 358.38 g/mol |
| Usnic_03 | *(R)*-1,1'-(7-benzyloxy)-3,9-dihydroxy-8,9b-dimethyl-1-oxo-1,9b-dihydrodibenzo[b,d]furan-2,6-diyl)bis(ethan-1-one) | 434.44 g/mol |
| Usnic_04 | *(R)*-1,1'-(7-benzyloxy)-3-hydroxy-9-methoxy-8,9b-dimethyl-1-oxo-1,9b-dihydrodibenzo[b,d]furan-2,6-diyl)bis(ethan-1-one) | 448.47 g/mol |
| Usnic_05 | *(R)*-1,1'-(7,9-bis-(benzyloxy)-3-hydroxy-8,9b-dimethyl-1-oxo-1,9b-dihydrodibenzo[b,d]furan-2,6-diyl)bis(ethan-1-one) | 524.57 g/mol |
| Usnic_06 | *(R)*-4,8'-diacetyl-7-hydroxy-2,9a-dimethyl-9-oxo-9,9a-dihydrodibenzo[b,d]furan-1,3-diyl-diacetate | 428.39 g/mol |
| Usnic_07 | *(R,E)*-6-acetyl-7,9-dihydroxy-8,9b-dimethyl-2-(1-(propylamino)ethylidene)dibenzo[b,d]furan-1,3-(2*H*,9b*H*)-dione | 385.42 g/mol |
| Usnic_08 | *(R,E)*-6-acetyl-2-(1-(benzylamino)ethylidene)-7,9-dihydroxy-8,9b-dimethyldibenzo[b,d]furan-1,3(2*H*,9bH)-dione | 433.46 g/mol |
| Usnic_09 | *(R,E)*-6-acetyl-3,7,9-trihydroxy-8,9b-dimethyl-2-(1-(phenylimino)ethyl)dibenzo[b,d]furan-1(9b*H*)-one | 419.43 g/mol |
| Usnic_10 | *(R)*-1,1'-(7-butoxy-3,9-dihydroxy-8,9b-dimethyl-1-oxo-1,9b-dihydrodibenzo[b,d]furan-2,6-diyl)bis(ethan-1-one) | 400.43 g/mol |
| Usnic_11 | *(R)*-1,1'-(9-butoxy-3,9-dihydroxy-8,9b-dimethyl-1-oxo-1,9b-dihydrodibenzo[b,d]furan-2,6-diyl)bis(ethan-1-one) | 400.43 g/mol |
| Usnic_12 * | *(R,Z)*-6-acetyl-2-(1-aminoethylidene)-7,9-dihydroxy-8,9b-dimethyldibenzo[b,d]furan-1,3(2*H*,9b*H*)-dione | 343.34 g/mol |
| Usnic_13 | 7-(Biotin-triazol-$PEG_4$)-usnic acid | 826.92 g/mol |

* Usnic_12 represents usenamine A from Yu et al. [3].

**Supplementary Table 2:** cryo-EM data table

| | **Class 1** | **Class 2** | **Class 3** | **Class 5** |
|---|---|---|---|---|
| Microscope | Titan Krios G3i | | | |
| Voltage [keV] | 300 | | | |
| Camera | Gatan K3 BioQuantum | | | |
| Magnification | 81,000 | | | |
| Pixel size at detector [Å/px2] | 1.07 | | | |
| Total electron exposure [e-/Å2] | 60 | | | |
| Number of collected frames [No.] | 54 | | | |
| Defocus range [µm] | -0.5 to -2.5 | | | |
| Energy filter slit width [eV] | 20 | | | |
| Automation software | Thermo Fisher EPU | | | |
| Micrographs collected [No.] | 7,595 | | | |
| Usnic acid [No.] | 3,608 | | | |
| Untreated [No.] | 3,987 | | | |
| Total extracted particles [No.] | 1,120,165 | | | |
| Final particle images [No.] | 79,656 | 144,717 | 183,665 | 99,866 |
| Treated particles [No.] | 55,651 | 138,233 | 16,408 | 5,626 |
| Untreated particles [No.] | 24,005 | 6,484 | 167,257 | 94,240 |
| Point-group symmetry | C1 | | | |
| Resolution global [Å] | 3.0 | 2.9 | 2.7 | 2.9 |
| Treated reconstruction [Å] | 3.0 | 3.0 | 3.7 | 3.7 |
| Untreated reconstruction [Å] | 3.0 | 3.4 | 2.6 | 2.7 |
| FSC-threshold | 0.143 | | | |
| Resolution range [Å] | 2.6 to 7.3 | 2.5 to 7.2 | 2.4 to 6.4 | 2.4 to 6.6 |
| Treated [Å] | 2.7 to 8 | 2.6 to 7.6 | 3.2 to 10.4 | 3.3 to 11.0 |
| Untreated [Å] | 2.7 to 9.3 | 3.1 to 11.9 | 2.4 to 6.5 | 2.4 to 6.6 |
| Plunging | Leica GP1 autofunction | | | |
| Grid type | 3.5/1 prefloated 2 nm carbon | | | |
| Adsorption time | 30 s | | | |
| Temperature and humidity | 4 °C, 75 % | | | |
| Blotting time | 2 s | | | |
| Volume | 4 µl | | | |
| Plotting | Frontside | | | |

**Supplementary Table 3**: Composition of the 4 Nsa1-TAP cryo-DRGN clusters (1-4).

| | | | cluster | | | |
|---|---|---|---|---|---|---|
| | **Description** | **UniProt** | **1** | **2** | **3** | **4** |
| **RNAs** | | | | | | |
| 25S | 25S ribosomal RNA | n.a | + | + | + | + |
| 5.8S | 5.8S ribosomal RNA | n.a | + | + | + | + |
| ITS2 | Internal Transcribed Spacer 2 | n.a. | + | + | + | + |
| **proteins** | | | | | | |
| Mak16 | Protein MAK16 | MAK16_YEAST | + | + | + | + |
| Rrp1 | Ribosomal RNA-processing protein 1 | RRP1_YEAST | + | + | + | + |
| Nsa1 | Ribosome biogenesis protein NSA1 | NSA1_YEAST | + | + | + | + |
| Rpf1 | Ribosome production factor 1 | RPF1_YEAST | + | + | + | + |
| Rrp14 | Ribosomal RNA-processing protein 14 | RRP14_YEAST | + | + | + | + |
| Rpl3 | 60S ribosomal protein L3 | RL3_YEAST | - | + | + | + |
| Rpl4A | 60S ribosomal protein L4-A | RL4A_YEAST | + | + | + | + |
| Rpl6A | 60S ribosomal protein L6-A | RL6A_YEAST | + | + | + | + |
| Rpl7A | 60S ribosomal protein L7-A | RL7A_YEAST | + | + | + | + |
| Rpl8A | 60S ribosomal protein L8-A | RL8A_YEAST | + | + | + | + |
| Rpl9A | 60S ribosomal protein L9-A | RL9A_YEAST | - | + | + | + |
| Ebp2 | rRNA-processing protein EBP2 | EBP2_YEAST | + | + | + | + |
| Cic1 | Proteasome-interacting protein CIC1 | CIC1_YEAST | + | + | + | + |
| Rpl13A | 60S ribosomal protein L13-A | RL13A_YEAST | + | + | + | + |
| Rpl14A | 60S ribosomal protein L14-A | RL14A_YEAST | + | + | + | + |
| Rpl15A | 60S ribosomal protein L15-A | RL15A_YEAST | + | + | + | + |
| Rpl16A | 60S ribosomal protein L16-A | RL16A_YEAST | + | + | + | + |
| Rpl17A | 60S ribosomal protein L17-A | RL17A_YEAST | + | + | + | + |
| Rpl18A | 60S ribosomal protein L18-A | RL18A_YEAST | + | + | + | + |
| Rpl20A | 60S ribosomal protein L20-A | RL20A_YEAST | + | + | + | + |
| Rpl21A | 60S ribosomal protein L21-A | RL21A_YEAST | - | - | - | + |
| Rpl23A | 60S ribosomal protein L23-A | RL23A_YEAST | - | + | + | + |
| Mrt4 | Ribosome assembly factor MRT4 | MRT4_YEAST | - | - | - | + |
| Rpl26A | 60S ribosomal protein L26-A | RL26A_YEAST | + | + | + | + |
| Brx1 | Ribosome biogenesis protein BRX1 | BRX1_YEAST | + | + | + | + |
| Nog1 | Nucleolar GTP-binding protein 1 | NOG1_YEAST | - | + | + | + |
| Rpl31A | 60S ribosomal protein L31-A | RL31A_YEAST | - | - | - | + |
| Rpl32 | 60S ribosomal protein L32 | RL32_YEAST | + | + | + | + |
| Rpl33A | 60S ribosomal protein L33-A | RL33A_YEAST | + | + | + | ` |
| Rpl35A | 60S ribosomal protein L35-A | RL35A_YEAST | + | + | + | + |
| Rpl36B | 60S ribosomal protein L36-B | RL36B_YEAST | + | + | + | + |
| Rpl37A | 60S ribosomal protein L37-A | RL37A_YEAST | + | + | + | + |
| Nip7 | 60S ribosome subunit biogenesis protein NIP7 | NIP7_YEAST | - | - | - | + |
| Nop7 | Pescadillo homolog (Nop7) | PESC_YEAST | + | + | + | + |
| Nop15 | Ribosome biogenesis protein 15 | NOP15_YEAST | + | + | + | + |
| Has1 | ATP-dependent RNA helicase HAS1 | HAS1_YEAST | + | + | + | + |
| Nop2 | 25S rRNA (cytosine(2870)-C(5))-methyltransferase | NOP2_YEAST | - | - | - | + |
| Nsa2 | Ribosome biogenesis protein NSA2 | NSA2_YEAST | - | - | - | + |
| Nug1 | Nuclear GTP-binding protein NUG1 | NUG1_YEAST | - | - | - | + |
| Rlp7 | Ribosome biogenesis protein RLP7 | RLP7_YEAST | + | + | + | + |
| Rlp24 | Ribosome biogenesis protein RLP24 | RLP24_YEAST | - | + | + | + |
| Nop16 | Nucleolar protein 16 | NOP16_YEAST | + | + | + | + |
| Erb1 | Ribosome biogenesis protein ERB1 | ERB1_YEAST | + | + | + | + |
| Tif6 | Eukaryotic translation initiation factor 6 | IF6_YEAST | - | + | + | + |
| Ssf1 | Ribosome biogenesis protein SSF1 | SSF1_YEAST | - | - | + | - |
| Rrp15 | Ribosomal RNA-processing protein 15 | RRP15_YEAST | - | - | + | - |
| Spb1 | 27S pre-rRNA (guanosine(2922)-2'-O)-methyltransferase | SBP1_YEAST | - | - | - | + |
| Rpl1A | Large ribosomal subunit protein uL1A | RL1A_YEAST | - | - | - | + |
| Dbp10 | ATP-dependent RNA helicase DBP10 | DBP10_YEAST | - | - | | + |
| Loc1 | 60S ribosomal subunit assembly/export protein LOC1 | LOC1_YEAST | - | - | - | + |
| YBL028C | Uncharacterized "UPF0642 protein YBL028C" | YBL028C_YEAST | - | - | - | + |

**Supplementary Table 4:** *Saccharomyces cerevisiae* strains

| ***S. cerevisiae* strain** | **genotype** | **source** |
|---|---|---|
| C303a | *MATa, ADE2, his3, leu2, trp1, ura3, can1-100* | Awad et al. [1] |
| C303a Rpl7a-GFP | *MATa RPL7A*-GFP*::HIS3*MX6*, ADE2, his3, leu2, trp1, ura3, can1-100* | Awad et al. [1] |
| C303a Rps9a-GFP | *MATa, RPS9A-GFP::HIS3MX, ADE2, his3, leu2, trp1, ura3, can1-100* | Awad et al. [1] |
| Nog1-GFP Nop58-mCherry | *MATa, leu2 ura3 his3 met15 NOG1-GFP::HIS3 NOP58-mCherry::hphNT1* | This study |
| Nog1-GFP Rpl7a-mCherry | *MATa; leu2; ura3; his3; trp1; RPL7A-mCherry::hphNT1; NOG1-GFP::HISMX* | This study |
| Tif6-GFP Hho1-mCherry | *MATα, leu2 ura3 his3 ade2 trp1 TIF6-GFP::HIS3 HHO1-mCherry::hphNT1* | This study |
| Bud20-GFP Nic96-mCherry | *MATa, leu2 ura3 his3 met15 BUD20-GFP::HIS3 NIC96-mCherry::hphNT1* | This study |
| Nop7-TAP | MATα, *leu2, ura3, his3, trp1, Nop7-TAP::TRP1* | Nissan et al. [4] |
| Nsa1-TAP | *MATα his3 leu2 ura3 trp1 Nsa1-TAP::TRP* | Ed Hurt |
| Noc2-TAP | *MATa his3 leu2 ura3 lys2 Noc2-TAP::URA3* | P. Milkereit |
| Bud20-GFP | *MATa ura3 leu2 his3 trp1 BUD20-TAP::HIS3* | This study |
| Nop53-GFP | *MATa leu2 ura3 his3 trp1 Nop53-TAP::HISMX* | This study |

**Supplementary Table 5:** Antibodies used in this study.

| primary antibody | dilution | source |
|---|---|---|
| α-Arx1 | 1:5 000 | M. Fromont-Racine |
| α-Cbp | 1:5 000 | Merck (cat-# 07-482) |
| α-Cic1 | 1:5 000 | University of Stuttgart |
| α-Crm1 | 1:10 000 | C. Yam |
| α-Ebp2 | 1:5 000 | M.A. McAlear |
| α-Erb1 | 1:5 000 | J. d. l. Cruz |
| α-Has1 | 1:5 000 | J. d. l. Cruz |
| α-Hrr25 | 1:5 000 | W. Zachariae |
| α-Mex67 | 1:10 000 | E. Hurt |
| α-Mtr4 | 1:1 000 | E. Hurt |
| α-Nmd3 | 1:4 000 | A. W. Johnson |
| α-Noc1 | 1:5 000 | P. Milkereit |
| α-Noc2 | 1:5 000 | P. Milkereit |
| α-Noc3 | 1:5 000 | P. Milkereit |
| α-Nog1 | 1:5 000 | M. Fromont-Racine |
| α-Nog2 | 1:5 000 | M. Fromont-Racine |
| α-Nop2 | 1:2 000 | Invitrogen (cat-# 10435964) |
| α-Nsa2 | 1:5 000 | M. Fromont-Racine |
| α-Nug1 | 1:10 000 | E. Hurt |
| α-Prp43 | 1:4 000 | E. Hurt |
| α-Rlp24 | 1:5 000 | M. Fromont-Racine |
| α-Rok1 | 1:5 000 | K. Karbstein |
| α-Rpp0 | 1:2 000 | J. Ballesta |
| α-Rpl16 | 1:40 000 | S. Rospert |
| α-Rrp12 | 1:5 000 | M. Dosil |
| α-Rsa4 | 1:10 000 | M. Remacha |
| α-Sof1 | 1:300 | E. Hurt |
| α-Ytm1 (Nop7) | 1:5 000 | J. d. l. Cruz |
| **secondary antibody** | **dilution** | **source** |
| α-rabbit | 1:15.000 | Sigma - Aldrich (cat-# A0545-1ML) |

**Supplementary Table 6:** Northern blot probes

| name | sequence (5´-3´) | binding site |
|---|---|---|
| 18S | CATGGCTTAATCTTTGAGAC | Mature 18S |
| 25S | CTCCGCTTATTGATATGC | Mature 25S |
| 5.8S | GCGTTCTTCATCGATGC | Mature 5.8S |
| 5S | GGTCACCCACTACACTACTCGG | Mature 5S |
| A2A3 | TGTTACCTCTGGGCCC | Between $A_2$ and $A_3$ cleavage site |
| EC2 | GGCCAGCAATTTCAAGTTA | Between E and $C_2$ cleavage site |
| DA2 | GACTCTCCATCTCTTGTCTTCTTG | Between D and $A_2$ cleavage site |

**Supplementary Table 7:** Absolute numbers of particles found in the 4 clusters of our cryoDRGN analysis in the combined, treated and untreated dataset. These numbers were used to calculate the percentage of total, which are depicted in Figure 5B.

| | | Cluster 1/No. particles | | | Cluster 2/No. particles | | |
|---|---|---|---|---|---|---|---|
| | | **Combined** | **Treated** | **Untreated** | **Combined** | **Treated** | **Untreated** |
| **batch** | **1** | 26,705 | 19,117 | 7,588 | 47,973 | 45,811 | 2,162 |
| | **2** | 26,559 | 18,342 | 8,217 | 48,955 | 46,781 | 2,174 |
| | **3** | 26,392 | 18,192 | 8,200 | 47,789 | 45,641 | 2,148 |

| | | Cluster 3/No. particles | | | Cluster 4/No. particles | | |
|---|---|---|---|---|---|---|---|
| | | **Combined** | **Treated** | **Untreated** | **Combined** | **Treated** | **Untreated** |
| **batch** | **1** | 60,998 | 5,361 | 55,637 | 33,625 | 1,927 | 31,698 |
| | **2** | 61,284 | 5,071 | 56,213 | 32,504 | 1,890 | 30,614 |
| | **3** | 61,383 | 5,976 | 55,407 | 33,737 | 1,809 | 31,928 |

## References Supplemental Information


1. Awad, D. *et al.* Inhibiting eukaryotic ribosome biogenesis. *BMC biology* **17,** 46; 10.1186/s12915-019-0664-2 (2019).
2. Zisser, G. *et al.* Viewing pre-60S maturation at a minute's timescale. *Nucleic acids research* **46,** 3140–3151; 10.1093/nar/gkx1293 (2018).
3. Yu, X. *et al.* Usnic Acid Derivatives with Cytotoxic and Antifungal Activities from the Lichen Usnea longissima. *Journal of natural products* **79,** 1373–1380; 10.1021/acs.jnatprod.6b00109 (2016).
4. Nissan, T. A., Bassler, J., Petfalski, E., Tollervey, D. & Hurt, E. 60S pre-ribosome formation viewed from assembly in the nucleolus until export to the cytoplasm. *The EMBO journal* **21,** 5539–5547; 10.1093/emboj/cdf547 (2002).